

Case Studies in Modelling Cruise-Generated Trailing Vortices

Anthony P. Brown*

*National Research Council Canada (NRC), Flight Research Laboratory,
U-61 Uplands, Ottawa, Ontario, K1A0R6, Canada*

Frank Holzäpfel†

*Deutsches Zentrum für Luft- und Raumfahrt, Institut für Physik der Atmosphäre,
82234 Oberpfaffenhofen, Germany*

<https://doi.org/10.2514/1.C038627>

Trailing vortices from jet transport aircraft in high altitude cruising flight, have been measured in high spatiotemporal detail, by a research jet operated by the National Research Council Canada. The vortex locations and circulations, descent rate and vortex core thermodynamic, dynamic, transport and spatial scale characteristics were derived. Also, from these measurements, the background atmospheric state properties of pressure, wind structure, temperature, thermal stratification and turbulence have been established. Selected cases from the measured data have been used to evaluate two versions of the Probabilistic 2-Phase (P2P) wake vortex prediction model. While the default P2P version uses ground-based measurement data to calibrate its probabilistic envelopes, the runtime optimized airborne version P2P^a uses uncertainties of all relevant impact parameters to construct the probabilistic envelopes. Flight and model data have been compared and the suitability of the P2P model versions for onboard wake vortex prediction and warning during cruise have been discussed.

Nomenclature

ABL	=	Atmospheric Boundary Layer
APA	=	AVOSS Prediction Algorithm
AVOSS	=	Aircraft Vortex Spacing System
b	=	geometric wingspan of the wake generator (m)
b_v	=	trailing pair vortex separation, lateral separation between centers (m)
CT-133	=	Canadair CT-133 Silver Star aircraft
DLR	=	Deutsches Zentrum für Luft- und Raumfahrt (German Aerospace Center)
D2P	=	Deterministic Two-Phase wake vortex prediction model
EDR	=	eddy dissipation rate (m^2/s)
g	=	gravitational acceleration (m/s^2)
L_t	=	integral turbulence length scale (m)
M	=	Mach Number (the quotient of true airspeed and the speed of sound)
N	=	Brunt-Väisälä frequency ($1/\text{s}$)
NASA	=	National Aeronautics and Space Administration

Presented as Paper 2024-3773 at the AIAA Aviation 2024 Forum, 29 July – 2 August, 2024.

* Research Pilot Engineer, CT-133 Facility Manager, Atmospheric Research Group, Anthony.Brown@nrc-cnrc.gc.ca, SMAIAA

† Senior Scientist, Applied Meteorology, frank.holzaeffel@dlr.de, Associate Fellow AIAA (Corresponding Author)

NRC	= National Research Council Canada
P2P	= Probabilistic Two-Phase wake vortex prediction model
P2P ^a	= airborne version of P2P model
PA	= pressure altitude (feet)
Δp	= flow angle surface pressure differential across two static holes, subtended asymmetrically by 50°
q	= turbulence velocity (m/s)
r_c	= vortex core radius, defined as the distance from vortex centre to peak tangential velocity (m)
s	= spanwise load factor
t	= time (sec)
t_0	= characteristic wake vortex timescale (sec)
T	= temperature (K); onset time of rapid decay (sec)
TASS	= Terminal Area Simulation System
TDAWP	= TASS Driven Algorithms for Wake Prediction
u	= headwind speed (m/s)
V_G	= true airspeed of the wake generating aircraft (m/s)
V_θ or V_T	= vortex induced tangential velocity magnitude (m/s)
v	= crosswind speed (m/s)
W	= weight of the trailing vortex generating aircraft (N)
w	= vortex descent speed (m/s); wind speed (m/s)
y	= lateral coordinate (m)
z	= vertical coordinate (m)
Γ	= trailing vortex circulation (m ² /s)
ε	= energy dissipation rate (m ² /s ³)
ν	= (effective) kinematic viscosity (m ² /s)
ρ	= atmospheric air density (kg/m ³)
σ	= standard deviation

Subscripts

e	= easterly
max	= maximum value
min	= minimum value
n	= northerly
0	= initial value
2	= second decay phase

Superscripts

*	= normalized quantity
---	-----------------------

I. Introduction

WAKE vortex research has largely been motivated by the operational problem of safely adjusting aircraft spacing to increase airport capacity and throughput [1]. But wake vortex encounters may also occur at cruise altitudes [2]-[5]. The encounter of a Bombardier Challenger CL604 of the wake of an Airbus A380-800 cruising 1000 feet higher in opposite direction in January 2017 received special attention, as the pilots of the CL604 recovered control only after a height loss of approximately 2700 m [6]. The Aviation Safety Reporting System (ASRS) associated 28% of wake vortex reports with takeoff and climb, 25% with cruise, and 47% with approach and landing in the United States airspace in a time frame between 1999 to 2009 [7].

The CT-133 research aircraft operated by NRC has been used extensively in the past for trailing vortex flight research [8]. During several flight tests the CT-133 has measured the dynamic, thermodynamic, and spatiotemporal characteristics, including vertical and lateral transport, of trailing vortices, generated by heavy jet transport aircraft in cruise flight. The environmental conditions were processed by excluding the wake vortex traverses from the measurement data.

The DLR has applied two versions of its fast-time wake-vortex prediction models to the flight measurement data. The fast-time wake models have been developed to evaluate newly proposed air traffic control and management procedures. These models take into account the varying atmospheric conditions and flight paths and can be used in predictive systems for the optimization of aircraft separations. A brief survey on the existing fast-time wake vortex models can be found in [1]. Both the ground-based and the airborne-based versions of the P2P model predict probabilistic envelopes of wake vortex transport and decay. The established Probabilistic 2-Phase wake vortex prediction model P2P is based on analytical considerations and large eddy simulations of different research groups and it is calibrated against data from wake vortex field experiments. The airborne version P2P^a minimizes the computational cost and uses the uncertainties of the relevant input parameters to derive the probabilistic envelopes.

To the authors' knowledge there are almost no publications presenting a detailed discussion of the prediction skills of fast-time wake vortex models in cruise conditions. Most published validation work of such models have employed data taken in the atmospheric boundary layer at low flight heights. NASA conducted flight tests with a Lockheed-Martin C-130 aircraft as vortex generator while NASA Langley's OV-10A was taking meteorological and wake vortex measurements mostly at test altitudes of 4000 or 5000 feet in 1995 and 1997 [9]. Two runs of flight 705 at an altitude of about 7500 ft were used to evaluate the performance of the fast-time wake vortex models APA [10] and TDAWP [11]. Deterministic and probabilistic predictions based on Monte-Carlo simulations of the wake vortex models were compared to the measurement data [12]. Further exceptions are the flight tests of DLR's wake encounter avoidance and advisory system (WEAA) using P2P^a [13] and the P2P simulations conducted in the framework of the unprecedented A380 test program [14], accomplished to determine appropriate separation standards for the A380 in the time frame from May 2005 to December 2007. Unfortunately, the latter P2P validations had to be treated as confidential and could not be published.

The current study fills an important gap in the evaluation of fast-time wake prediction models under cruise conditions. As wake vortex physics is usually modelled as a kinematic problem, the substantial differences of air density in the atmospheric boundary layer (ABL) and at cruise altitude shouldn't play a role. To first order aircraft are just flying faster at high altitudes to compensate for the lower air density leading to similar values of initial wake vortex circulation. The ranges of the relevant environmental parameters prevailing in the ABL and at tropopause altitudes overlap widely [15]. While the ranges of thermal stratification appear quite similar, one may expect on average higher values of atmospheric turbulence and wind shear in the ABL. In contrast, the higher wind speeds at cruise altitude may lead to much larger wake vortex transport distances. In ground proximity the interaction of the trailing vortices with the ground may dominate wake behavior. As wake vortex physics would not differ fundamentally between the different flight altitude ranges, the challenge of wake vortex prediction at cruise rather lies in the appropriate treatment of the uncertainties of the environmental and aircraft parameters needed as inputs to the wake vortex predictions, which may be much harder to estimate and higher for cruise conditions than close to an airport.

Three case studies are presented in this paper which evaluate the fast-time model predictions using the flight test data. The case studies include wake vortices generated by an A380, on the 15th March 2012, by an A359, on the 14th January 2019, and by a B744, on the 19th October 2018. The three cases were selected according to the following criteria: they should preferably contain a high number of vortex traverses covering a substantial range of vortex ages, and the investigated flight segments should be straight without maneuvers in a preferably homogeneous atmospheric environment. The impact of the input parameters on the wake vortex prediction quality and the limitations they impose on operational applications are discussed. An earlier version of this paper was presented at the AIAA Aviation 2024 Forum [16].

II. Experimental details

The NRC measurement aircraft (Fig. 1) was fitted with 600 Hz inertial and air data sampling, processing and recording. Two cm diameter cylinders with boundary layer transition-fixing strips were installed for the instantaneous measurement of surface-flow, which are used for the derivation of vortex-induced flow angles. The differential surface pressure was measured with the help of high-rate pressure transducers, which sensed surface Δp across two tiny static holes, separated by an asymmetric subtended angle of 50° across the cylinder surface. In the vortex crossplane (plane orthogonal to the trailing vortex axis), 600 Hz sampling resulted in a Nyquist spatial scale of a few centimeters. Inertial data was sensed by an adjacent inertial measurement unit in the nosebay. Differencing of the true airspeed vector (transformed through Euler angles, to the earth axis system) and inertial vector resulted in the derivation of the instantaneous wind vector. Extraction of the mean wind resulted in the derivation of the vortex-induced airflow velocity.



Fig. 1 NRC CT-133: underwing instrumentation pods (*left*); close-up view (*right*) shows the nose boom with pitot-static tube, and crossflow cylinders for flow angle measurement.

Flight profiles consisted of air traffic control vectored interception of Heavy Category jet transport aircraft flying enroute at heights of 10-12 km, in vortex condensate conditions (vortex core condensate, Figs. 2 and 3 prevailed as far as vortex lengths of 30-40 km). Wake vortex projects 2006-2021 [8] generally employed vortex core penetrations from below, *i.e.* six o'clock position (see Figs. 2 right and 3 right). By this technique, the greatest amount of individual trailing vortex core state characteristic data was obtained, from which vortex core states of varying core radii, velocity maxima and vorticity concentrations have been obtained. From this entry position, it was possible to remain in vortex cores for times up to 0.6-1.2 second duration.



Fig. 2 A380 intercept at 3 km (*left*), apparent curvature is a camera focal length effect; at ≈ 20 km (*right*), vortices in asymmetric state.



Fig. 3 A359 intercept at 5 km distance (*left*), and in the vortex pair, at 15 km distance (*right*).

III. The Probabilistic Two-Phase Wake Vortex Model Versions P2P and P2P^a

The Probabilistic Two-Phase wake vortex decay and transport model (P2P) was developed, in the first instance, to guide the safe readjustment of aircraft separations during approach and landing. Later it was also applied successfully to departures and cruise. For such applications a fast-time wake vortex prediction model must be capable of providing accurate and reliable predictions of vortex position and strength in real time. P2P considers all effects of the leading order impact parameters: aircraft configuration (span, weight, speed, heading, flight path angle), as well as the environmental parameters of wind (cross and head components), wind shear, turbulence, temperature stratification, and proximity of the ground. The model predicts the deterministic (mean) evolution (Deterministic Two-Phase model D2P) together with envelopes for vortex trajectories and strengths with specified probabilities (P2P model). The model design rests on four pillars: dimensional analysis, the equation for the laminar decaying potential vortex, the adjustment to large eddy simulation results of different groups, and the calibration with field experiment data. The design, applications, and validation activities of P2P are described in detail in a series of Journal publications [17]-[20]. In total the P2P model has been validated against in ground effect and out of ground effect measurement data of four US and more than ten European field measurement campaigns employing over 16,000 individual cases. The field experiment data used for model calibration was gathered during measurement campaigns conducted at airports [19] where both aircraft parameters and meteorological parameters can be obtained with significantly higher accuracy than at cruise altitudes. So, it is expected that the probabilistic envelopes will not be sufficiently wide for the current application of cruise flight.

The airborne model version P2P^a was tailored to the requirements of real-time airborne wake vortex prediction [13]. For this purpose, the dynamical core of the Probabilistic Two-Phase wake vortex model P2P has been retained. P2P^a focuses the modelling effort and the related computation effort on the most important impact parameters identified in a previous sensitivity study [15]. The model design distinguishes between (i) the parameters that can be modelled by the superposition of the variances of the uncertainties of the input parameters and (ii) the parameters that can only be considered via the non-linear model equations. The former approach (i) refers to the spreading of the envelopes of wake vortex position caused by uncertainties of wind, wind shear, turbulence, aircraft position, and ground altitude. The latter approach (ii) considers the effects on both vortex decay and vortex transport which are affected by the parameters that define initial vortex circulation (mass, speed, span, air density), wingspan, turbulence and temperature stratification. Off-line Monte Carlo simulations are used to adapt the probabilistic model output to envelopes of 90%, 95%, and 99% probabilities. For a prescribed probability level this allows a reduction of internal model iterations to four by employing four dedicated combinations of the parameters initial vortex separation, b_{v0} , initial vortex circulation, Γ_0 , Brunt-Väisälä frequency, N , energy dissipation rate, ϵ , onset time of rapid vortex decay, T_2^* , and kinematic viscosity during rapid vortex decay, ν_2^* . These four runs yield minimum wake vortex descent

distance, z_{min} , maximum vortex descent distance, z_{max} , minimum vortex lifetime, t_{min} , and maximum vortex lifetime, t_{max} .

Independent from the respective probability level, effects of vortex deformation are added to lateral and vertical spreading. For this purpose, an expression based on the amplitude growth of the Crow instability following Ref. [21] is used. The ambient atmospheric turbulence causes scatter in the wake vortex positions which is modelled assuming that the RMS value of ambient turbulence is superimposed on the propagation velocity [19]. Here it is anticipated that the turbulence velocity may transport the vortices in a single direction during a whole wake vortex lifetime because the energy containing eddies of the atmosphere are typically larger than the wake vortices ($L_t > b_0$). The turbulence velocity is estimated from the dissipation rate following [22]. For the average dissipation rate of $5.5 \cdot 10^{-6} \text{ m}^2/\text{s}^3$ in cruise conditions reported by [23] the turbulence velocity amounts to 0.17 m/s. P2P^a employs the maximum of the formula from [22] and a background turbulence velocity set to 0.1 m/s. For vortex scatter in the vertical direction, the P2P^a model employs 50% of the lateral position uncertainties [19].

IV. Measurement Results and Discussion

Background atmospheric data is required as state input data to the P2P models, namely 3-D winds, thermal stratification, and turbulence dissipation rate against pressure altitude. Many figures depicting meteorological parameters in the subsections below include flight segments containing traverses through wake turbulence. These segments are identified and excluded postflight to obtain background atmospheric data.

A. A388 case, flight data

1. Stratification and turbulence

Flight data soundings indicated atmospheric conditions consisted of light turbulence in terms of eddy dissipation rate, EDR, and mostly neutral thermal stratification shown in terms of a Brunt-Väisälä frequency squared, N^2 in Fig. 4.

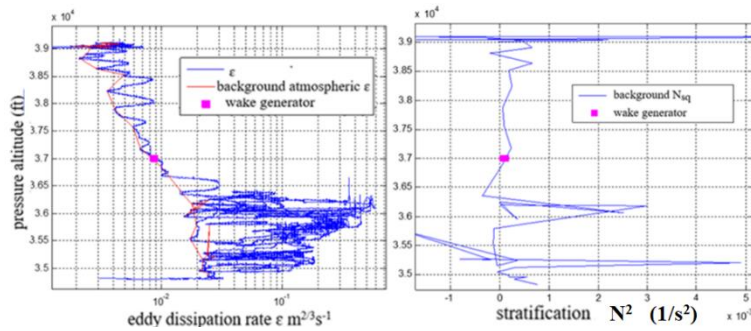


Fig. 4 Eddy dissipation rate (left) and stratification (right), neutral at generator height; wake generator height 11,091 m, with atmospheric temperature lapse rate correction included.

2. Pressure, temperature and winds

The soundings of P, T and winds are presented in Fig. 5, together with the perturbations upon these quantities, induced by the trailing vortex pair. It is seen that windspeed was reasonably constant, but backed in direction to the north with increasing height. Typical vortex-induced perturbation velocities were of the order of 20 m/s, to maxima of 35 m/s. The wake vortices were typically warmer than background, by as much as 3.5 K. The A388 was 600 m below the onset of the tropopause. In the wake vortex cores, pressure reductions of 0.5-0.7 kPa were measured.

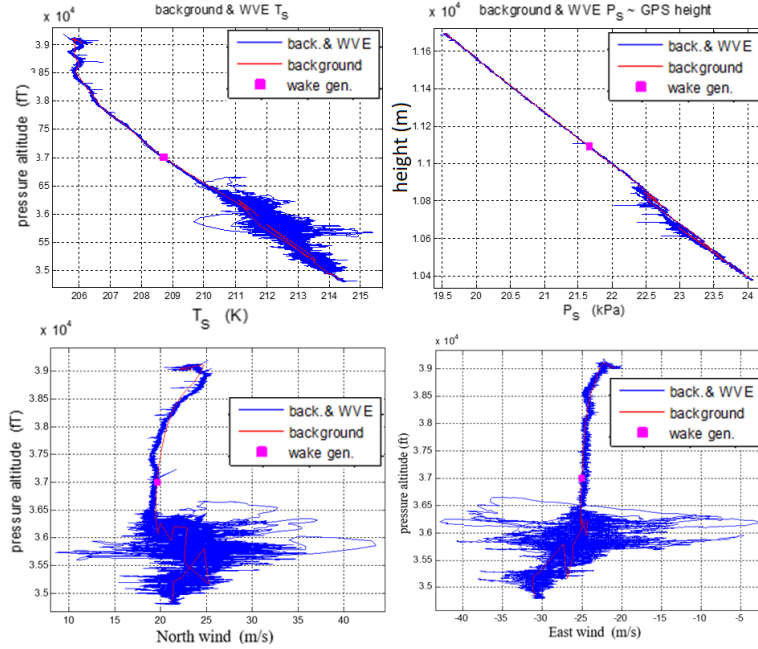


Fig. 5 In-situ atmospheric soundings: (*top row*), air temperature (*left*), air pressure (*right*), (*bottom row*), north and east wind components.

3. Flight data of vortex generation and transport

At vortex generation altitude, atmospheric conditions were air temperature 214.8 K, air pressure 21.665 kPa (at pressure altitude of 37,000 feet) and air density 0.3617 kg/m^3 . The A388 mass was 495,010 kg and flying at 0.86 M, equating to 252 ms^{-1} . Derived optically *via* perspective analysis of video records similar to Figs. 2 *left* and 3 *left* (but directly in-trail, thereby negating the optical curvature), the vortex spacing, b_{v0} , was estimated to be approximately 52.7 m (or 65.8% of geometric span). A vortex circulation of $\Gamma = 1,011 \text{ m}^2\text{s}^{-1}$ was calculated from the estimated vortex spacing b_{v0} . This data was used for the P2P initializations. The trailing vortex induced velocity field for 50-60 sec vortex age, has been re-constructed from port and starboard vortex core traverses, Fig.6, showing vortex cross-plane tilt of $\approx -30^\circ$ and somewhat reduced vortex spacing, implying a degree of circulation asymmetry and long-wave excitation.

Trailing vortex transport is depicted in Fig. 7. Concerning vertical transport, the first vortex core traverse was conducted at a wake length near 10 km (approximately 45 sec age, non-dimensional wake time $t^* \approx 2.6$). For modelling vortex descent, the accuracy of the vortex generation height must be considered, which for a pressure altitude of 37,000 feet, will vary with the temperature profile of the atmosphere.

During the trailing vortex intercept descent (between 12-17 km wake length), the GPS-referenced height of a pressure altitude of 37,000 feet was measured by the CT-133, as $11.091 \pm 0.023 \text{ km}$. However, the height accuracy of the generator aircraft was unknown. It can be bounded by the RVSM standard deviation, σ of 31 m. The global height-keeping performance by ICAO [24][15] specifies height-keeping errors beyond 90 m (300 ft) in magnitude to less than 0.002. Assuming a Gaussian distribution, the 0.002 probability corresponds to 2.9 standard deviations, and thus one standard deviation is estimated to 31 m. This bias error on wake generator height would track through the P2P solution; albeit an initializing error, rather than a solution confidence limit.

Each vortex core traverse defines the vertical position of the vortex core at that position. It is seen that the vertical vortex path was generally non-linear, but varied harmonically, with variable amplitude and period. The non-linear amplitude was greatest between 35 and 45 km trailing vortex length.

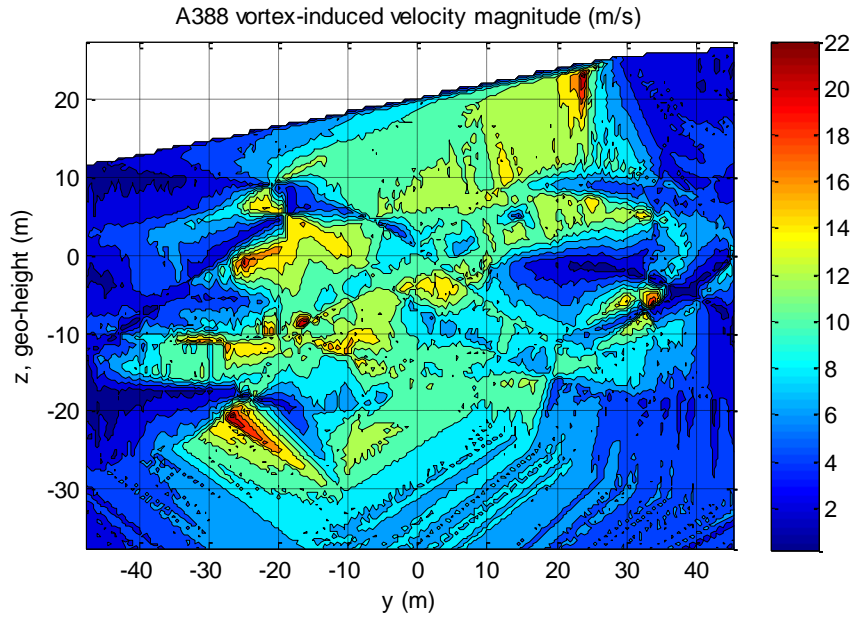


Fig. 6 Re-constructed crossplane vortex velocity field at 50-60 s age, from a concatenated number of vortex core traverses (red patches).

The lateral transport of the vortex pair (Fig. 7) contained differences to the wind-drift transport at descending vortex height. The differences are possibly due to the interaction of background atmospheric shear with vortex transport. The vortex crossplane background shear $\omega_{YZi} = \Delta_i w_Z / \Delta_i y - \Delta_i w_Y / \Delta_i z$ was represented by the flight data approximation of quasi-vorticity, which was a sequential spatial forward-differencing of wind component magnitudes, and had the underlying assumption that temporal variations were significantly lower than spatial velocity gradients at the CT-133 flight speed of Mach 0.6. Thus derived, the quasi-vorticity sounding is shown in Fig. 7, lower right. In the light background atmospheric turbulence at generator height, it was low, $< 1 \text{ s}^{-1}$, increasing above and below the generator. Within the trailing vortex flowfield, patches of quasi-vorticity of $10\text{-}100 \text{ s}^{-1}$ were present.

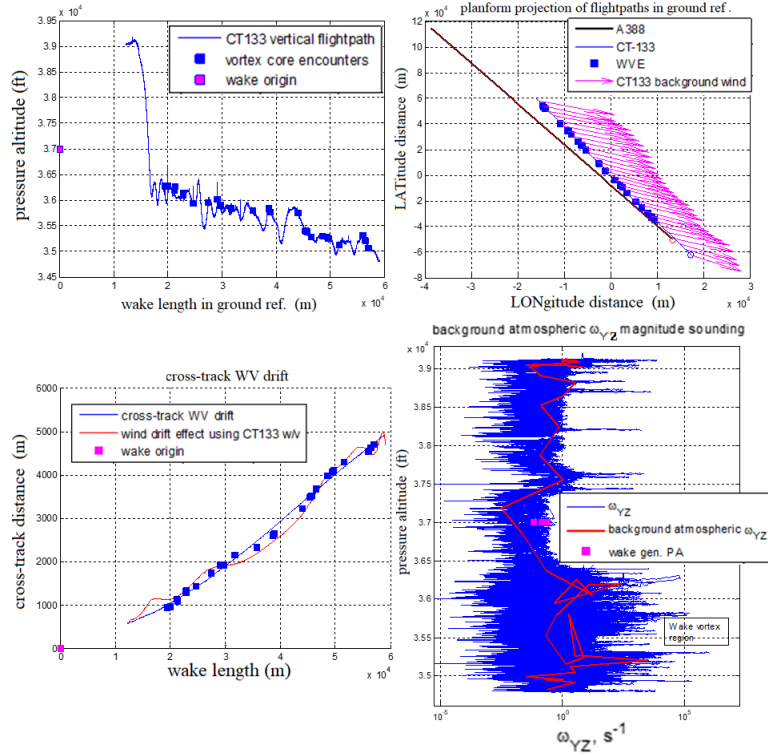


Fig. 7 Trailing vortex transport: (top row) vertical (left) and lateral (right); (bottom row) lateral transport (left) separating wind drift and vortex drift, (right) sounding of quasi-vorticity.

B. A359 case, flight data

1. Background stratification and turbulence

The A359 wake survey was conducted north of Ottawa, Ontario. The generating aircraft was tracking northwest from a departure airport on the North American northeastern seaboard. Thus, the wake survey was conducted close to the top-of-climb, with the A359 in a heavy fuel-load state. As shown in Fig. 8, the background atmospheric conditions at the generator height of 10.15 km, consisted of light stratification and light turbulence.

2. Pressure, temperature and winds

The soundings of measured P, T and winds for the A359 case are presented in Fig. 9, together with the perturbations upon these quantities, induced by the trailing vortex pair. Down-track, the easterly wind component, w_e , increased in magnitude, whilst in the sounding maneuver both the northerly and easterly components reduced in magnitude with increasing altitude. Typical vortex-induced perturbation velocities were of the order of 20 m/s. The wake vortices were both warmer and cooler than the background, as much as +2/-3 K. In the wake vortex cores, decreases in pressure of 0.2-0.5 kPa were measured.

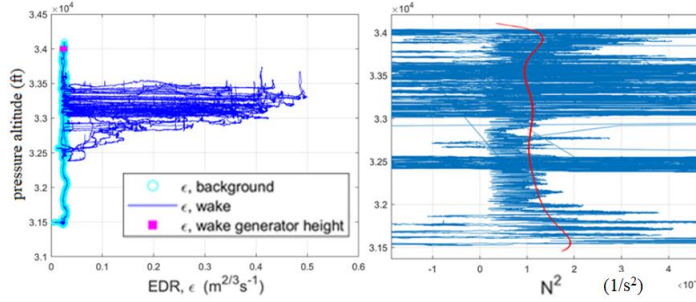


Fig. 8 Soundings of atmospheric turbulence (EDR, *left*) and stratification (*right*), A359 flight data; wake generator height 10,150 m, with atmospheric temperature lapse rate correction included.

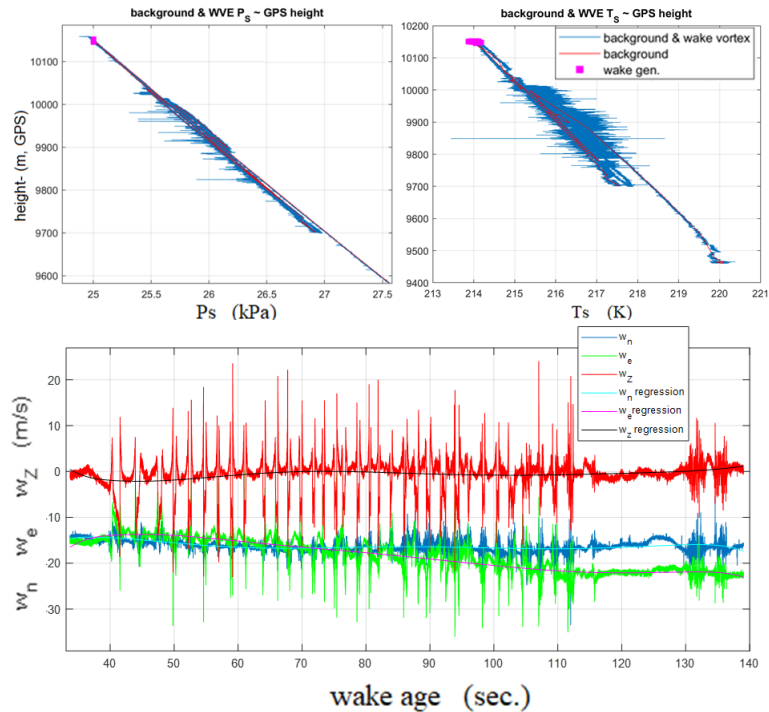


Fig. 9 Soundings of atmospheric pressure (*top left*), temperature (*top right*) and time traces of wind components (*bottom*), A359 flight data.

3. Flight data of vortex generation and transport

Principally, lateral traverses of the A359 vortex pair were flown, Fig. 10, together with a vertical sounding towards the end of the survey. The measured vertical component of vortex velocity is included in Fig. 10, highlighting the lateral movement of peak velocity (+20 m/s) location, induced by vortex meandering with 40–45 m vortex spacing and long-wave excitations. The behavior of vortex spacing with age and varying background ϵ is depicted in Fig. 11, including photographs of vortex state. b_V was measured two ways: optically using a perspective analysis of the splay angle between port and starboard vortices, in the video record of condensate trails, and directly, for the lateral traverses of the CT-133 across the vortex pair. ϵ varied between 0.024 and 0.05 $\text{m}^{2/3}/\text{s}$, in small-scale turbulence and larger scale shear, respectively, with a mean value of approximately 0.03 $\text{m}^{2/3}/\text{s}$. The vortex descent path is depicted in Fig. 12, together with the lateral drift of the vortex pair, which is the combination of background atmospheric wind drift and atmospheric shear, or other interaction generally.

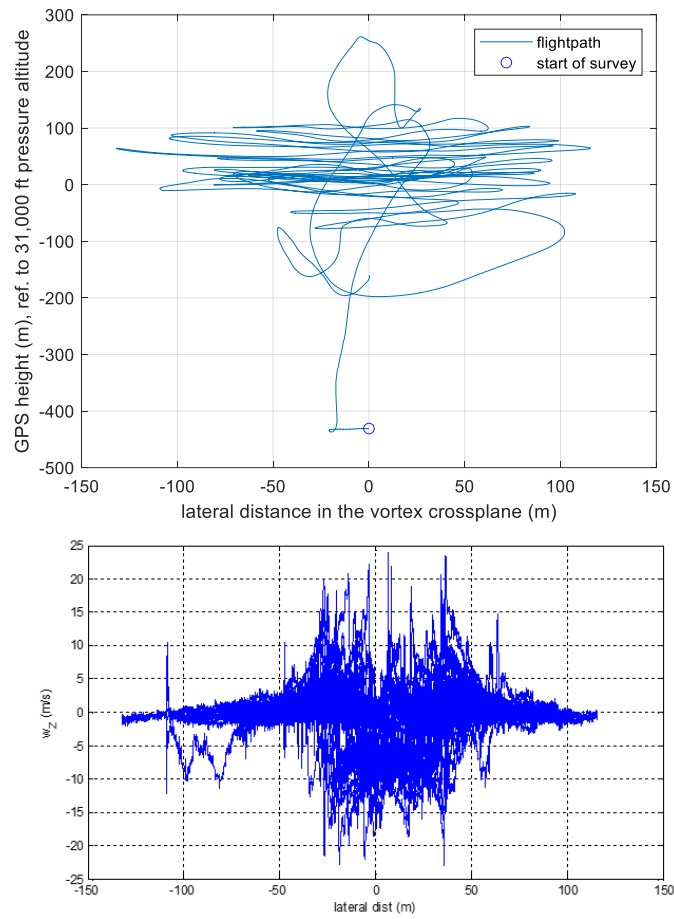


Fig. 10 Vortex crossplane flightpath ensemble (*top*), wake age 40-114 sec; ensemble of vortex core traverse vertical winds (*bottom*).

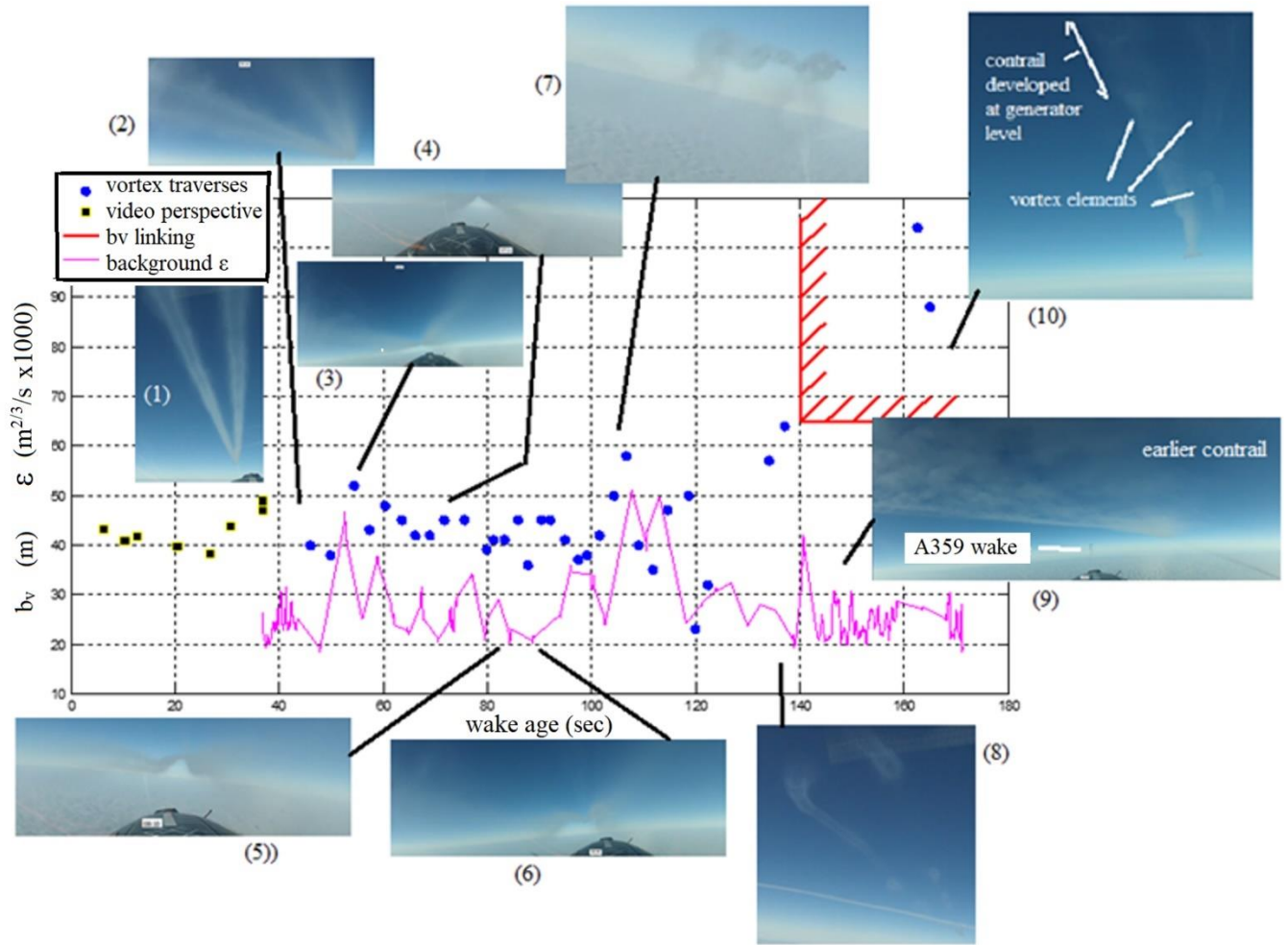


Fig. 11 Vortex separation, b_v and EDR, ϵ , plotted against wake age.

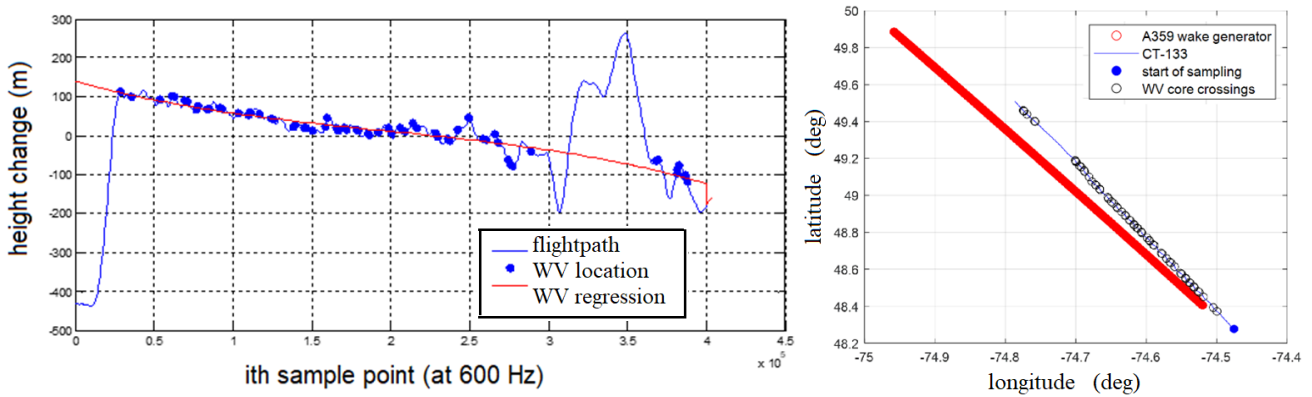


Fig. 12 A359 trailing vortex descent path (*left*); planform view of A359 and CT-133 flightpaths (*right*), depicting effects of wind drift and atmospheric interaction, upon WV transport.

C. B744 case, flight data

1. Background stratification and turbulence

The B744/CT-133 flight data was gathered during a wake turbulence research flight, 19th October 2018. The flight occurred north of Ottawa, Ontario. As encountered by the CT-133, ϵ is presented in Fig. 13, together with a magnified plot of stratification. Background ϵ varied between approximately 0.03 and 0.05 $\text{m}^{2/3}/\text{s}$. The atmosphere was lightly stratified, an N^2 of 0.0005 s^{-2} at generator height, and neutral to lightly stratified below.

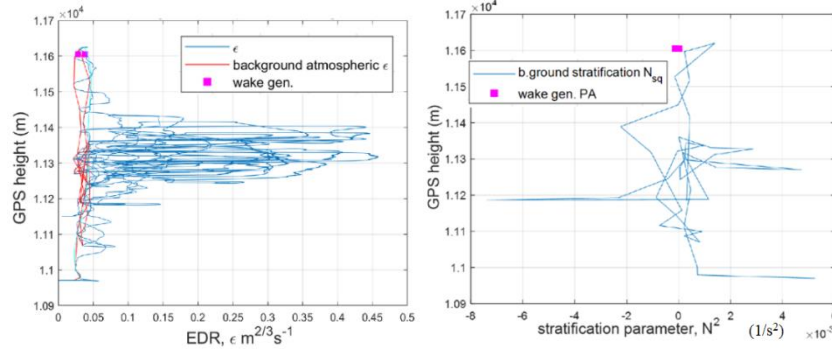


Fig. 13 B744 flight case, atmospheric turbulence (including WV) and stratification, as encountered by the CT-133.

2. Pressure, temperature and winds

Soundings of P, T and northerly/easterly wind components are shown in Fig. 14. It is seen that the trailing vortices were generated in the upper troposphere at approximately 11,605 m height. The background temperature lapse rate was slightly non-linear, tropopause onset was possibly 11,230 m. Vortex core-induced pressure expansions were 0.4 to 0.8 kPa, whilst the cores were up to 4 K warmer than background, generally, with some cool segments, 1 K cooler than background. The mean values of northerly and easterly background wind components had approximately zero lapse rate for the upper 150 m of the sounding. In the lower half of the sounding, magnitude was also similar, but the wind direction backed to the west, with reducing height. Vortex induced wind magnitude variations were as much as $\pm 25 \text{ m/s}$.

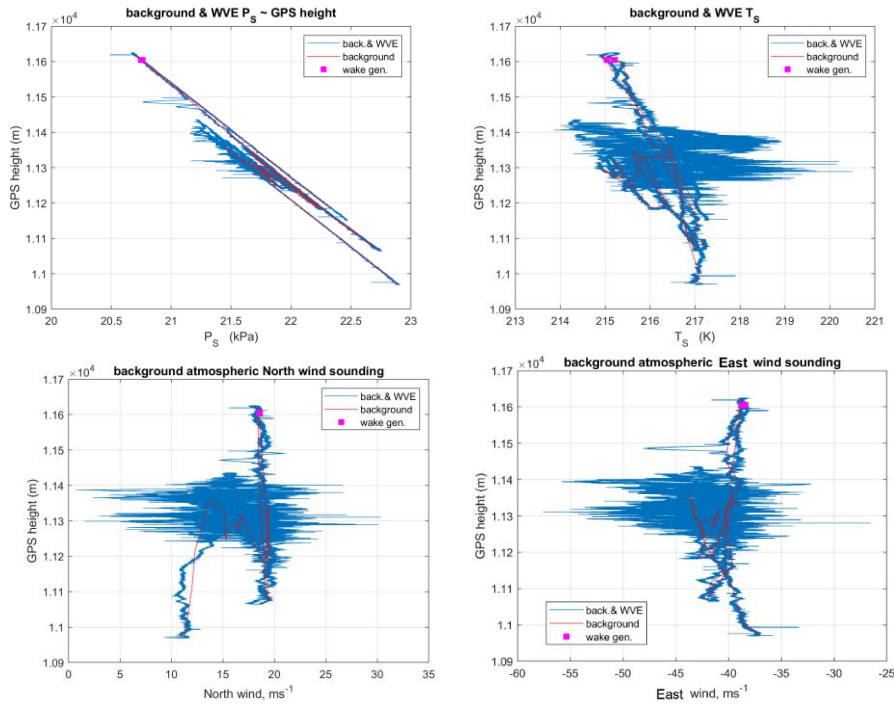


Fig. 14 B744 flight case, soundings of atmospheric pressure, temperature (*upper plots*) and horizontal winds (*lower*); wake generator height approximately 11,605 m.

3. Trailing vortex generation and transport

Trailing vortex generation is pictorially shown in Fig. 15. From a number of B744 cruising flight wake vortex flight surveys at 0.84-0.86 M, mean measured b_V was 42 m ($0.65b$). Using this value for b_{V0} trailing vortex circulation at generation was calculated to be $686 \text{ m}^2/\text{s}$.

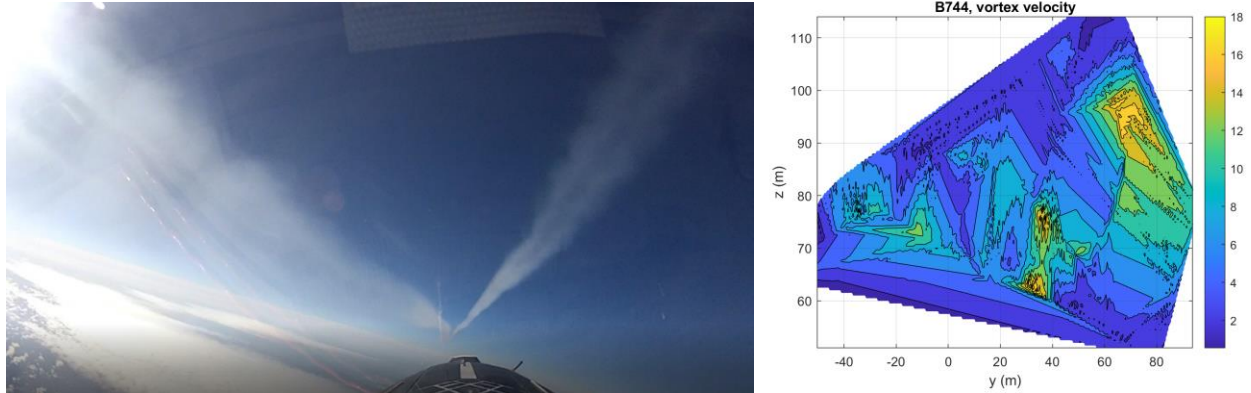


Fig. 15 B744 trailing vortices from generation to age 50 sec (*left*); contour plot of vortex velocity magnitude from a number of core traverses (*right*).

The trailing vortex descent path, as described by the set of vortex core traverse points, is shown in Fig. 16. It is seen that there were deviations from a constant vortex descent rate, with localized excursions, prevalently upwards. The vortex core traverses have been analyzed as gust rise and fall events, Fig. 17. The rise/fall plot identified two vortex modes, 10 m/s at the spatial scale of about 3 m, and 15 m/s at a spatial scale of 9 m. An example of the larger spatial scale is also shown in Fig. 17 right, for which the core structure appeared to have been asymmetric, circumferential vortices of the smaller scale size, with a vented core interior between them. The asymmetry suggested an unsteady, transformational vortex state around the core circumference, between core entry and core exit.

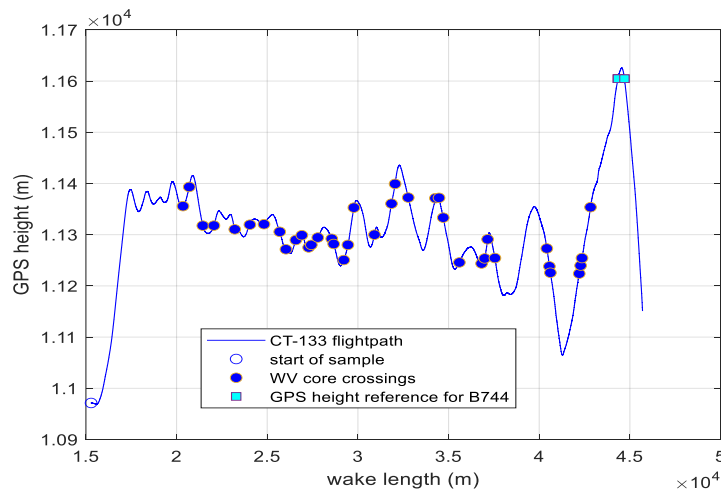


Fig. 16 Descent path of the B744 trailing vortices, ascertained from vortex core traverse positions.

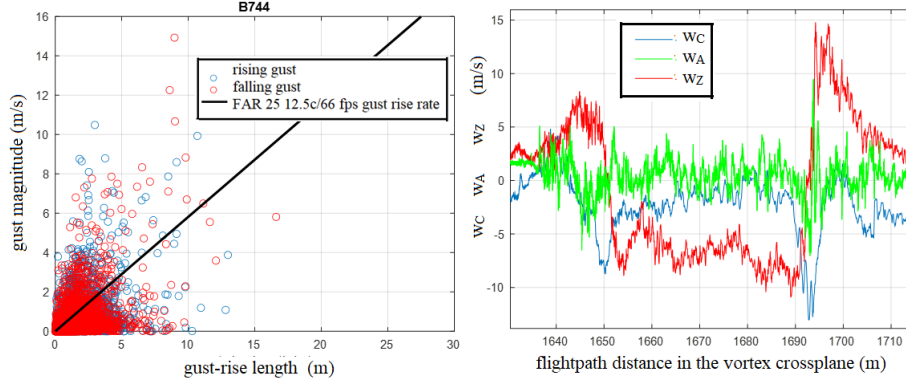


Fig. 17 B744 trailing vortex traverses, expressed as gust rise and fall magnitudes (*left*) and the vortex velocity components from a singular traverse through the pair (*right*).

V. P2P and P2P^a wake vortex predictions

A. A388 case – predictions with ground-based P2P model

The comparison of the P2P predictions with the CT-133 wake vortex measurements of the A388 case is shown in Fig. 18. The vertical profiles of the meteorological input data, in the height range where the wake vortices evolve, stem from all the CT-133 measurements in the relevant height range, irrespective from the locations where the measurements have actually been taken. As these also include measurements at similar altitudes but quite remote locations down-track, the profiles partly exhibit substantial jumps which are most pronounced for energy dissipation rate, ϵ . As P2P employs running averages for the environmental data controlling wake vortex decay [17] (turbulence and thermal stratification), the scatter of this data is tolerable for the P2P prediction quality. Average values of energy dissipation rate and of Brunt-Väisälä frequency within the height range from vortex generation down to the lowest measurements amount to $\epsilon = 9.4 \cdot 10^{-6} \text{ m}^2/\text{s}^3$ and $N = 0.0042 \text{ 1/s}$, respectively. For cruise conditions this corresponds to moderate turbulence and very weak thermal stratification [15]. The scatter of the wind data, however, would introduce layers with apparent quite pronounced wind shear. Therefore, the wind shear parameterization of P2P [19] has been deactivated for this assessment. Vortex age is computed from the measured vortex length by dividing it by the true airspeed of the A380 of 252 m/s. So, headwind transport of the wake vortices has not to be considered explicitly.

In Fig. 18 the mean (deterministic) vortex behavior is denoted by red and green lines for the port and starboard vortices, respectively, while the probabilistic envelopes are blue for the 2- σ allowances. In the upper left plot for vortex descent, the CT-133 measurements are distributed around the lower probabilistic envelope. An initial circulation of $\Gamma = 1011 \text{ m}^2/\text{s}$ was calculated from the estimated vortex spacing, $b_{v0} = 52.7 \text{ m}$, yielding the notably small characteristic vortex time scale $t_0 = 17.3 \text{ s}$ and also a notably high initial descent speed of $w_0 = 3.1 \text{ m/s}$. As the descent speed is well met until a vortex age of about 125 s, the estimated initial values for the circulation and vortex separation appear reliable.

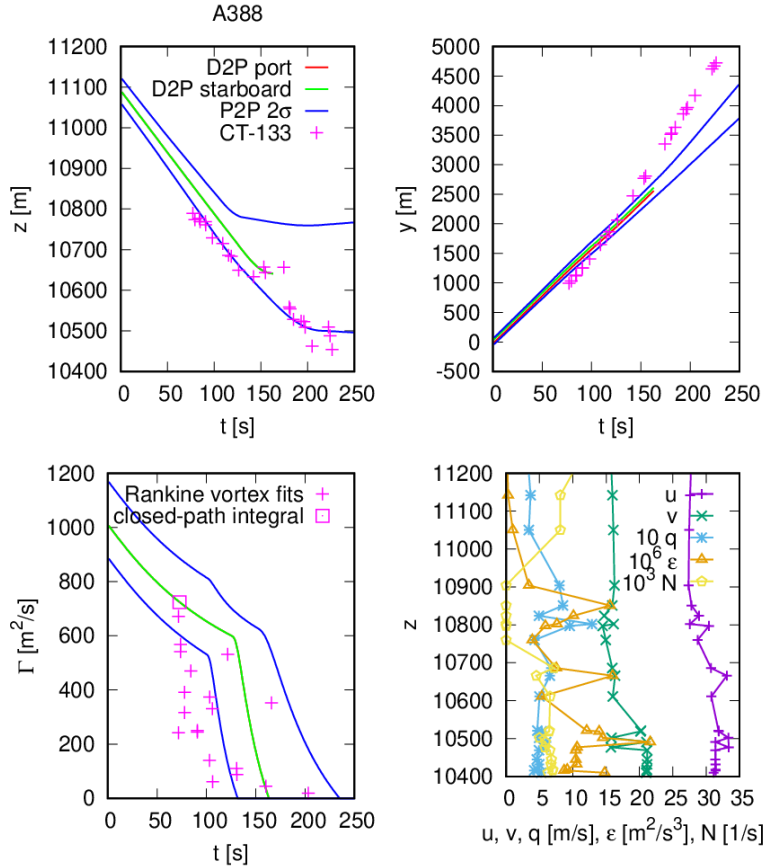


Fig. 18 Trailing vortex evolution of A388 aircraft measured by CT-133 (magenta symbols) and predicted with P2P model (lines) using measured initial vortex separation of 52.7 m.

One may argue that the estimated flight altitude of the A388 may be a little too high. Reducing the vortex generation altitude by only 50 m yields a perfect agreement of the measured and predicted deterministic vortex descent (not shown). So, the 50 m offset is well within the uncertainty of $\sigma = 31$ m estimated from the global height-keeping performance by ICAO [24], even when the altitude uncertainties of the CT-133 are neglected. Note that the measured vortex descent distance is remarkably high covering 637 m. Even if the possibly lower flight altitude of the A388 is considered, the vortex descent distance is still on the order of 2000 ft and thus twice the reduced vertical separation minimum (RVSM) of 1000 ft. Note that the P2P model has been trained employing measurement data collected in ground proximity, where most parameters and in particular flight altitude feature substantially smaller uncertainties compared to experiments conducted in cruise conditions.

The lateral vortex drift prediction (Fig. 18 top, right) appears to be close to the measurements. The lateral drift increases in both measurement and prediction when the vortices descend into regions with increasing crosswind at 10,600 m altitude at a vortex age of about 150 s. However, the crosswind transport is somewhat underestimated and the probabilistic envelopes are far too narrow. Again, it should be stated that the model uncertainties are tailored to measurement data collected in ground proximity, where crosswind estimates are more accurate and the resulting predicted probabilistic envelopes are substantially narrower.

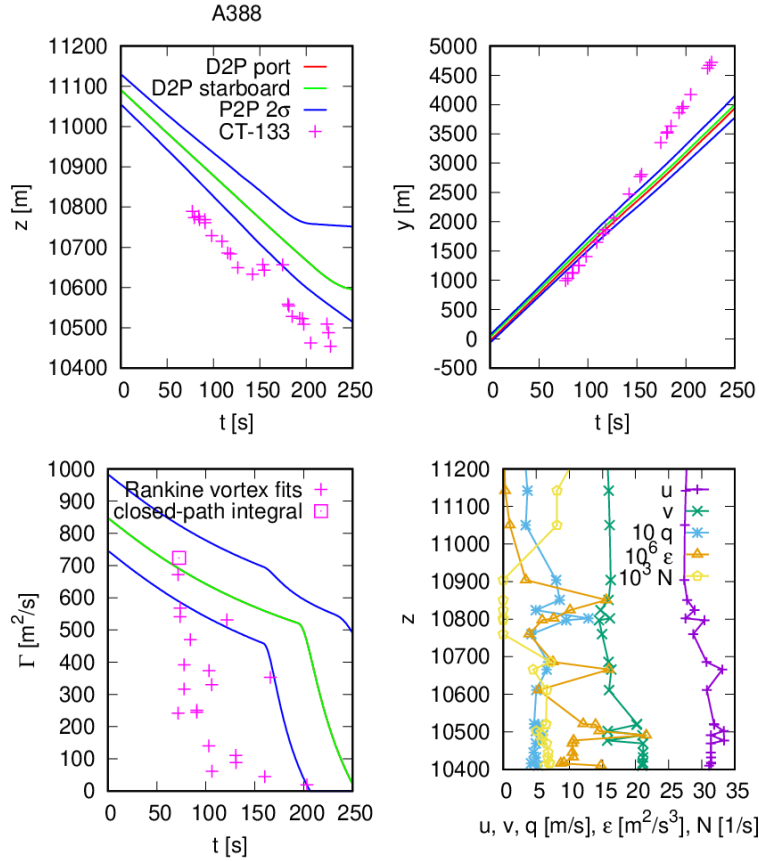


Fig. 19 Trailing vortex evolution of A388 measured by CT-133 (symbols) and predicted with P2P (lines) with initial vortex separation of 62.8 m for elliptical circulation distribution.

Fig. 18 bottom left illustrates estimates of vortex circulation using either fits of the Rankine vortex model to the measured vortex velocities or from flying a closed-path integral around a vortex together with the corresponding circulation predictions. For the Rankine vortex fit, first, the vortex center is determined assuming rotational symmetry of the vortex and linear tangential velocity profiles within the core radius. Then the velocity profiles of the advance towards the vortex center and the recede from the center are translated into two tangential velocity profiles to which a Rankine velocity profile is fitted by optimization of the values for vortex core radius and circulation. Note that the vortex properties may change along the flightpath with a typical length of 150 m needed for crossing a vortex with a typical diameter of 10 m which will unavoidably translate into uncertainties of the circulation estimates.

In Fig. 18 bottom left the closed-path integral resides exactly on the green curve for deterministic circulation decay. All circulation measurements are well covered by the upper bound of the predicted probabilistic envelopes while the rapid decay apparently sets in earlier in the observations than in the predictions. The predicted deterministic vortex lifetime of 163 s appears reasonable as it corresponds to 9.4 vortex time scales, t_0 , given the low value of $t_0 = 17.3$ s. Potentially, after this vortex rings are forming that can be measured until a vortex age of 226 s ($13 t_0$) which is slightly shorter than the maximum predicted 2- σ envelope for circulation reaching until 234 s.

Fig. 19 illustrates vortex predictions assuming elliptical circulation distribution leading to an initial circulation of $\Gamma_0 = 848 \text{ m}^2/\text{s}$ and an initial vortex spacing of $b_{v0} = 62.8 \text{ m}$ yielding a vortex time scale of $t_0 = 29.2 \text{ s}$ and an initial descent speed of $w_0 = 2.1 \text{ m/s}$. Now, even the deterministic vortex lifetime lasts with 254 s longer than the vortex

observations. However, due to the much smaller initial descent speed the observed vortex descent speed and descent distance are clearly underestimated.

B. A388 case – predictions with airborne P2P^a model

The input parameters employed for the wake vortex predictions with the airborne P2P^a model are listed in Table 1. For all parameters an estimate of the average value and a respective standard deviation is prescribed. Additionally, for wind, turbulence, and thermal stratification the respective vertical gradients are included. For the latter meteorological parameters, the average values on flight altitude and their standard deviations as well as the vertical gradients are derived from linear fits to the measurement data gathered by the CT-133.

Fig. 20 shows the comparison of the P2P^a predictions with the CT-133 wake vortex measurements of the A388 case. For the uncertainty allowances a 95% probability has been selected. Fig. 20 bottom right depicts the meteorological parameters as used by the four internal P2P^a prediction runs. For every meteorological parameter at least one vertical profile for minimum values and one for maximum values are generated to support the prediction of the envelopes of the vortex parameters with the selected 95% probability.

For illustration purposes, the plots of vortex position and strength also comprise the results of the four internal P2P^a runs denoted z_{min} , z_{max} , t_{min} , and t_{max} . For vortex circulation, Γ , shown in Fig. 20 bottom left, these runs define directly the blue probabilistic envelopes, while for vortex position the curves produced by the internal runs are expanded by superposition of the variances of various relevant input parameters.

A comparison of Fig. 18 and Fig. 20 clearly elucidates that the uncertainty allowances of the airborne version P2P^a are substantially larger than those of the ground-based P2P. As a consequence, all the measurements for vortex descent reside within the probabilistic envelope of P2P^a while for lateral transport this is mostly the case with the exception of a period ranging from 77 s to 91 s. The 95% envelopes for circulation well encompass the Rankine vortex fits.

Table 1 Input parameters for P2P^a for A388 case

parameter	value	standard deviation	gradient
mass	495010 kg	4950 kg	-
vortex separation	52.7 m	4.7 m	-
true airspeed	252 m/s	2 m/s	-
true heading	338.4°	1°	-
altitude	11091 m	31 m	-
air density	0.362 kg/m ³	0.001 kg/m ³	-
wind speed	29.6 m/s	1.1 m/s	-0.0129 1/s
wind direction	124.2°	2.6°	-9.26·10 ⁻⁴ °/m
energy dissipation rate	2.38·10 ⁻⁶ m ² /s ³	4.22·10 ⁻⁶ m ² /s ³	1.83·10 ⁻⁸ m/s ³
potential temperature	324.7 K	0.27 K	1.90·10 ⁻³ K/m

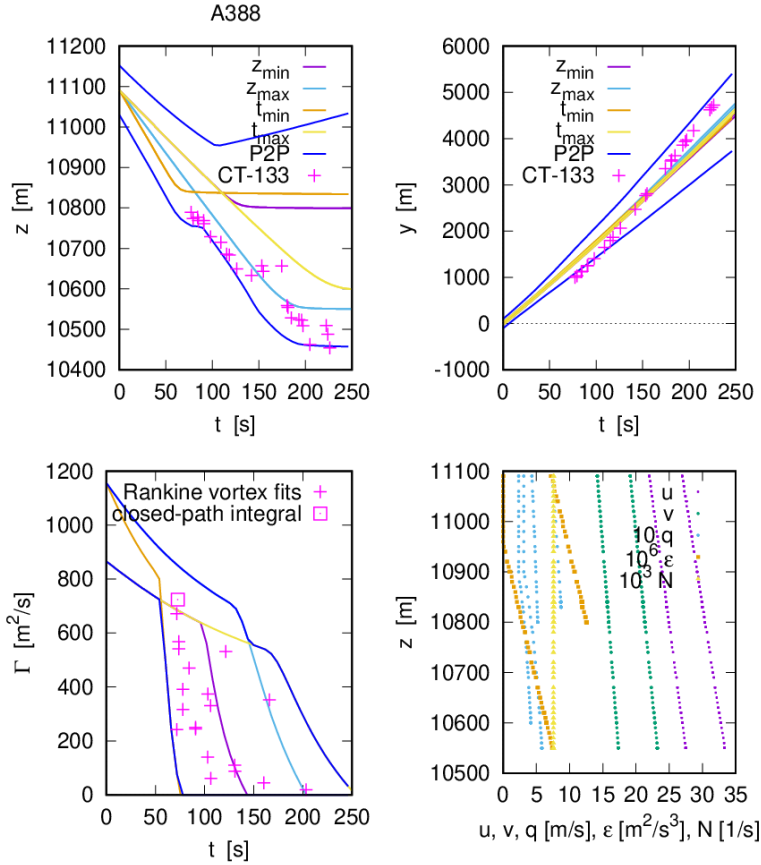


Fig. 20 Trailing vortex evolution of A388 aircraft measured by CT-133 (symbols) and predicted with airborne P2P^a model (lines) using measured initial vortex separation of 52.7 m.

Fig. 21 illustrates the P2P^a predictions assuming elliptical circulation distribution with an initial vortex spacing of $b_{V0} = 62.8$ m (wingspan $b = 79.75$ m) and without any standard deviation. First of all, it is noticeable that with zero standard deviation of the initial vortex separation the runs for z_{min} , t_{min} and z_{max} , t_{max} almost fall on top of each other, respectively, while the lifetime range is increased compared to the case employing the smaller initial b_{V0} of the more compact measured vortex pair. Again, like in Fig. 19 for P2P, the much smaller descent speed does not meet the observed vortex descent speed and yields a substantially smaller descent distance. Combining the elliptical b_{V0} with a standard deviation that would enclose the observed descent distances, would yield excessively large probabilistic envelopes. The comparison to the circulation estimates based on the observations indicates that vortex lifetime is somewhat overestimated using the assumption of elliptical circulation distribution.

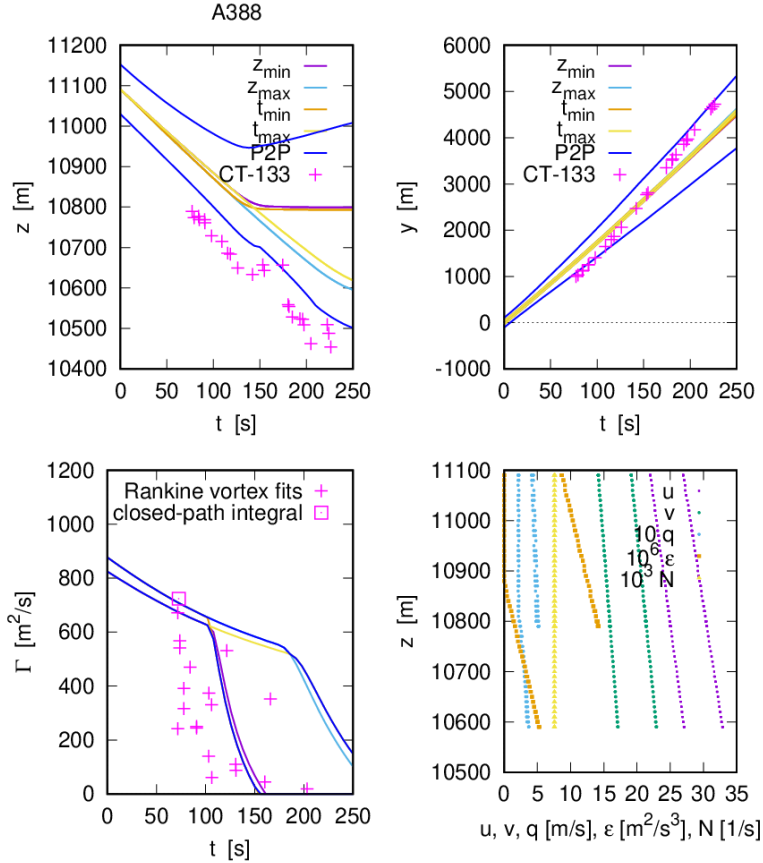


Fig. 21 Trailing vortex evolution of A388 aircraft measured by CT-133 (symbols) and predicted with airborne P2P^a model (lines) using elliptical initial vortex separation of 62.6 m.

C. A359 case – predictions with ground-based P2P model

Fig. 22 depicts the P2P predictions of the evolution of the wake vortices generated by the A359 aircraft together with the underlying CT-133 measurements. The predictions are initialized with a vortex separation of $b_{V0} = 43.4$ m which is an average of measurements taken between vortex ages from 10 s to 100 s and an initial circulation of 585 m²/s estimated from flight data. Average values of energy dissipation rate and of Brunt-Väisälä frequency within the height range of measured vortex evolution amount to $\varepsilon = 1.3 \cdot 10^{-5}$ m²/s³ and $N = 0.0081$ 1/s, respectively. Again, this corresponds to moderate turbulence and quite weak thermal stratification for cruise conditions [15]. The comparison of predictions with measurements yields a quite similar picture as for the A388 case such that many comments made in sections V.A and V.B also hold here.

Again, the measured vortex descent is distributed around the lower 95% envelope. With a decrease of the A359 flight altitude of only 50 m, the measurements would be equally distributed around the deterministic prediction (green line) except the late measurements after 122 s (not shown). The late vortex altitude measurements feature substantial height variations indicating that the sinusoidal deformation of Crow instability [25] or even the subsequent stage of the formation of vortex rings has set in. Again, as for the A388, using the initial separation of $b_{V0} = 50.9$ m, resulting from the assumption of an elliptical circulation distribution, yields a clear underestimation of the descent speed (not shown).

The uncertainty allowances for lateral vortex position appear far too small. Also, the lateral transport resulting directly from the crosswind profiles features opposite trends of measurement and prediction; at a vortex age around

70 s the lateral transport speed is increased in the measurements while it is reduced in the predictions. So, although the mean lateral transport speed is well met, there is substantial uncertainty in the crosswind field, which is not considered adequately by the P2P model calibrated with measurement data collected in ground proximity at airports. The circulation estimates from the measurements in Fig. 22 left bottom vary within quite broad limits at given vortex ages, while most estimates are situated even below the deterministic circulation predictions.

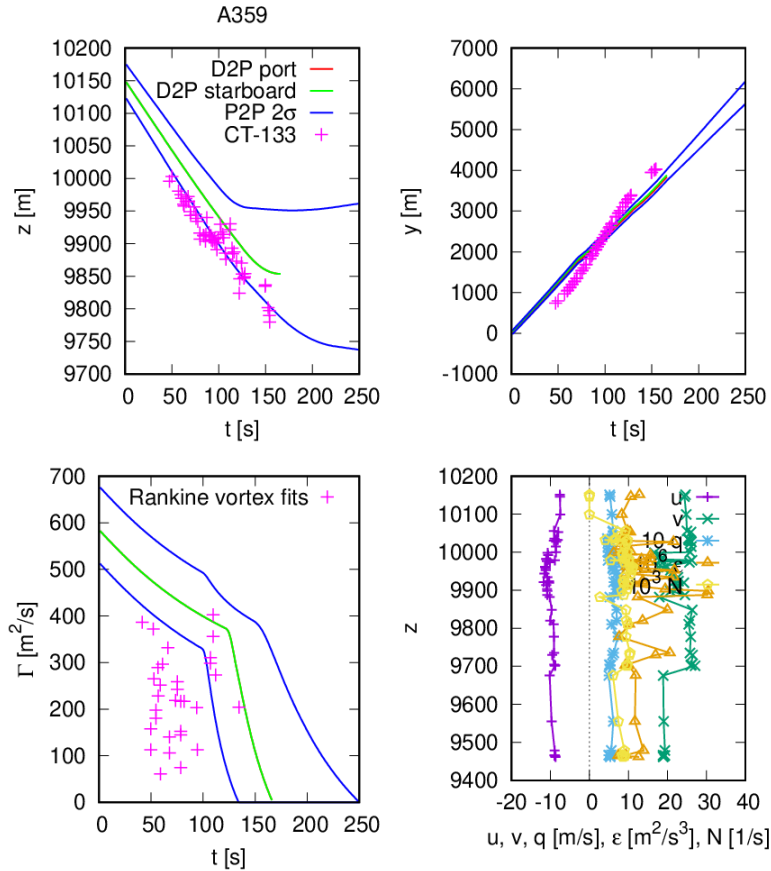


Fig. 22 Trailing vortex evolution of A359 aircraft measured by CT-133 (symbols) and predicted with P2P model (lines) employing measured initial vortex separation of 43.4 m.

D. A359 case – predictions with airborne P2P^a model

Fig. 23 shows the comparison of the P2P^a predictions with the CT-133 wake vortex measurements of the A359 case. The input parameters employed for the wake vortex predictions with the airborne P2P^a model are listed in Table 2. Using the standard deviations of the input parameters derived from the scatter of the measurement data, almost all measured vortex positions reside within the probabilistic envelopes. The lower probabilistic envelope for vortex descent just encloses the measured descent distances, while the descent speeds seen in the measurements and the predictions correspond very well. With a descent distance of 370 m also the wake vortices generated by the A359 reach the next flight level 1000 ft below, even when the uncertainties of the flight altitudes are considered. The envelopes for lateral transport mostly enclose the measurement data thanks to the high standard deviations of wind speed and direction even though the average lateral transport speed is not so well met and the model design does not foresee nonlinear vertical wind gradients. Parts of the Rankine vortex circulation estimates reside below the lower probabilistic envelope while the upper more relevant envelope appears adequate.

Altogether, the P2P^a model design appears to be well-suited to deal with the substantial uncertainties of the input parameters as they typically occur during cruise operations. One example of how the model copes with these uncertainties, which appears not so successful in this case though, is the increase in the upper probabilistic envelope for vertical position after 90 s. This increase is caused by the quite high standard deviations of wind speed and direction, as these could also be related to substantial vertical wind shear that might trigger vortex rebound [26], [27] which, however, is not the case here.

Table 2 Input parameters for P2P^a for A359 case

parameter	value	standard deviation	gradient
mass	256240 kg	2560 kg	-
vortex separation	43.5 m	3.2 m	-
true airspeed	243.4 m/s	2 m/s	-
true heading	342.4°	1°	-
altitude	10150 m	31 m	-
air density	0.407 kg/m ³	0.0025 kg/m ³	-
wind speed	25.5 m/s	2.6 m/s	0.00241 1/s
wind direction	49.4°	5.4°	-0.000926 °/m
energy dissipation rate	9.58·10 ⁻⁶ m ² /s ³	5.77·10 ⁻⁶ m ² /s ³	-2.28·10 ⁻⁸ m/s ³
potential temperature	319.2 K	0.181 K	0.0037 K/m

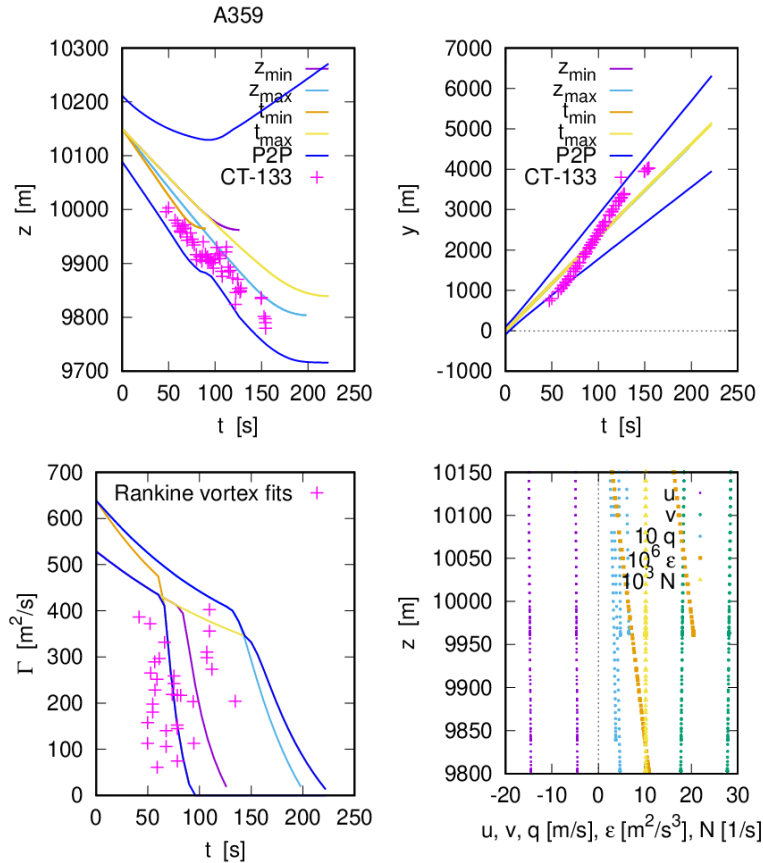


Fig. 23 Trailing vortex evolution of A359 aircraft measured by CT-133 (symbols) and predicted with airborne P2P^a model (lines) using initial values listed in Table 2.

E. B744 case – predictions with ground-based P2P model

Fig. 24 depicts the P2P predictions of the B744 case together with the corresponding CT-133 measurements. The predictions were initialized with the measured initial vortex separation of $b_{v0} = 41.9$ m, which for the Boeing aircraft is even 17.2% smaller than the theoretical value of $b_{v0} = 50.6$ m for elliptical circulation distribution. From all the considered cases the B744 case features the highest values of the atmospheric turbulence and stratification, which are controlling vortex decay, with average values around $\varepsilon = 4.6 \cdot 10^{-5} \text{ m}^2/\text{s}^3$ and $N = 0.017 \text{ 1/s}$. While the degree of stable thermal stratification still appears typical for the tropopause region, the atmospheric turbulence is slightly increased [15]. Also, the crosswind around 42 m/s is quite strong.

Despite the highest values for turbulence and thermal stratification, the measured vortex lifetime corresponds to remarkable 172 s and the vortex descent of 382 m still clearly exceeds the reduced vertical separation minimum of 1000 ft. The P2P predictions underestimate vortex descent by up to almost 50 m which could be attributed to an overestimation of the vortex generation altitude (Fig. 24, top left). On the other hand, the measured and predicted spreads of vertical vortex positions are matching well. As can be seen on a video taken during the flight, the reduced descent distances of the vortices between vortex ages of 120 s to 140 s in a height range between 11350 m and 11400 m can be attributed to partly extreme vortex pair tilting of up to 90° tilt angles, which may greatly reduce or even completely suppress vortex descent. Vortex tilting is observed for pronounced vertical gradients of crosswind shear [26], [27], as evidenced in the height range between 11,460 m and 11,500 m, where the wind fluctuations are not related to wake vortex crossings (see Fig. 14 bottom). The use of the initial vortex separation for elliptical circulation distribution of $b_{v0} = 50.6$ m instead yields a substantially smaller initial vortex descent speed, such that most measured vertical vortex positions are found below the corresponding probabilistic envelope (not shown).

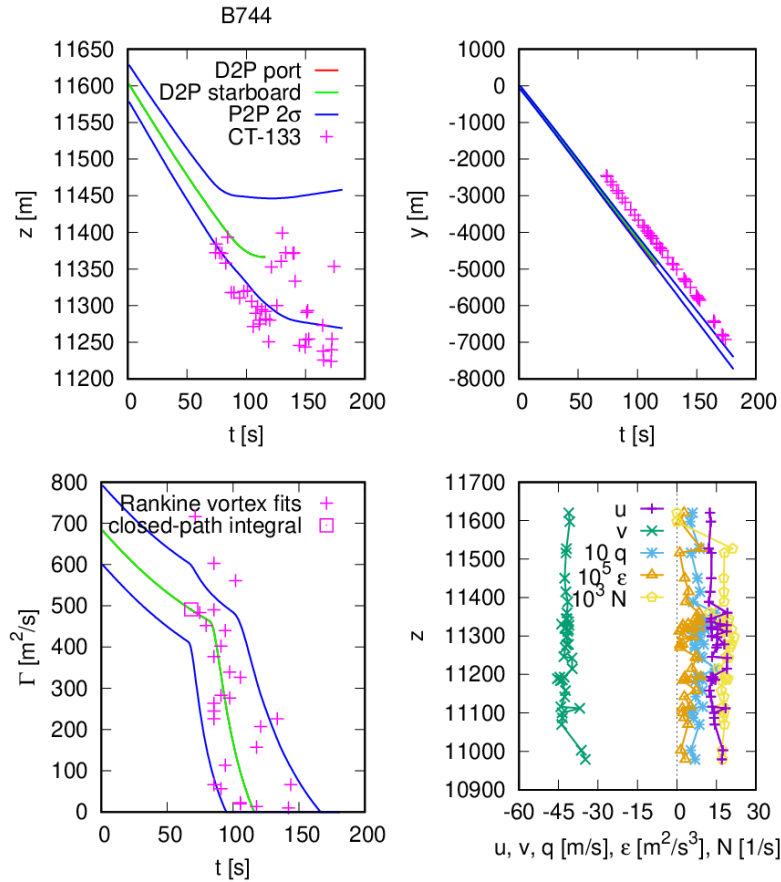


Fig. 24 Trailing vortex evolution of B744 aircraft measured by CT-133 (symbols) and predicted with P2P model (lines) using measured initial vortex separation of 41.9 m.

Measured and predicted lateral vortex transport feature similar slopes but no overlap. It appears that the crosswind experienced by the vortices during the early vortex descent was lower than the crosswind reconstruction from the complete CT-133 flight, where the crosswinds used for the prediction of the early vortex descent were gathered only towards the end of the chase flight (see Fig. 16). This change of wind direction along the CT-133 flight is most obvious in the lower northerly winds prevailing during the early aircraft measurements shown in Fig. 14 bottom left. The wind field in the B744 case is an example where the assumption of homogeneous atmospheric conditions during the wake vortex observations comes to its limits. Clearly, the spread of the probabilistic envelopes of the ground-based P2P model is not sufficiently wide to include the aircraft measurements under these conditions. Fig. 24 bottom left indicates that the predicted deterministic onset time of rapid circulation decay at a vortex age of approximately 85 s and the slope of the subsequent rapid decay (green line) are well in line with the Rankine vortex-based circulation estimates (magenta symbols). Also, the majority of the measured circulation values is well covered by the predicted probabilistic envelopes with the exception of a few quite high circulation values.

F. B744 case – predictions with airborne P2P^a model

Fig. 25 compares P2P^a predictions with the measurements employing the input data listed in

Table 3. As, in contrast to the previous cases, the gradient of potential temperature corresponds to substantial stable thermal stratification, also a standard deviation of 20% of the temperature gradient corresponding to 0.021 K/m has been prescribed.

The measured vortex descent including its spread is well covered by the 95% probabilistic envelopes, where the initial descent speeds of the four internal P2P^a runs varies between 2.4 m/s and 3.4 m/s. Wake vortex lifetime is slightly underestimated possibly related to the small characteristic vortex time scales, t_0 , between 11 s and 16 s resulting from the small initial b_{v0} of 41.9 m as well as the stable thermal stratification. Nevertheless, most circulation measurements are situated well within the predicted 95% envelopes.

However, also P2P^a does not meet the measured lateral vortex transport due to the inhomogeneous wind field as discussed in the previous section. While the first vortex measurement at 74 s is off by 400 m from the 95% envelope, this distance decreases over time to 65 m for the measurement at 150 s. An adjustment of the specified uncertainties in order to completely cover the observed lateral vortex transport may be achieved for example by tripling the standard deviation of the wind speed to 4.29 m/s. So, the B744 example highlights the importance of as precise as possible environmental data to correctly predict vortex transport within reasonably small bounds.

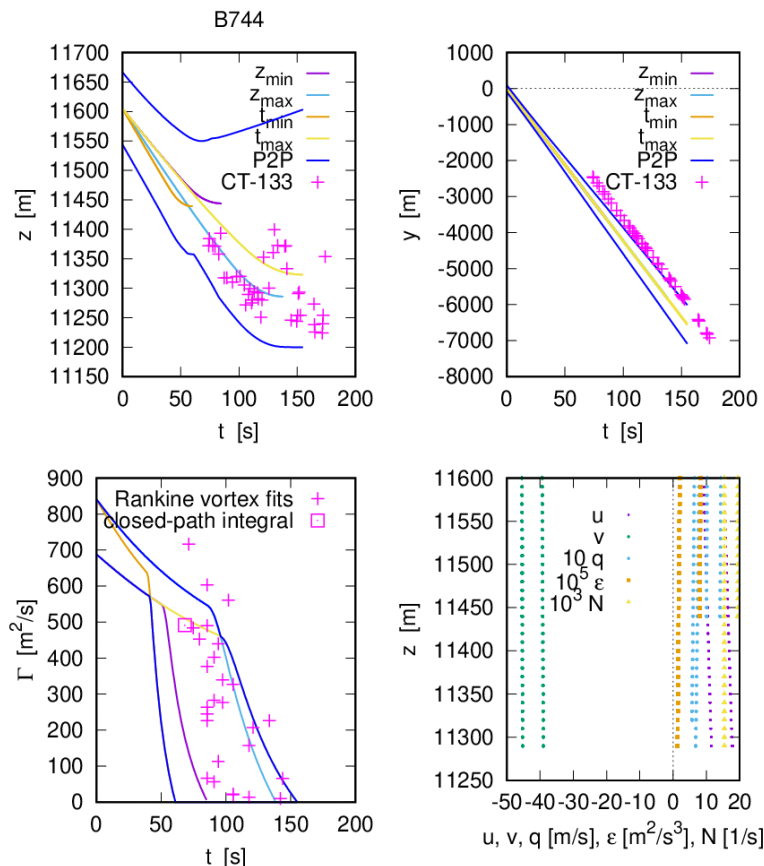


Fig. 25 Trailing vortex evolution of B744 aircraft measured by CT-133 (symbols) and predicted with airborne P2P^a model (lines) using initial values listed in

Table 3.

Table 3 Input parameters for P2P^a for B744 case

parameter	value	standard deviation	gradient
mass	270000 kg	2700 kg	-
vortex separation	41.9 m	3.2 m	-
true airspeed	246 m/s	4 m/s	-
true heading	222.3°	0.4°	-
altitude	11605 m	31 m	-
air density	0.3361 kg/m ³	0.0002 kg/m ³	-
wind speed	44.1 m/s	1.43 m/s	-0.00153 1/s
wind direction	116.3°	3.35°	0.00994 °/m
energy dissipation rate	5.16·10 ⁻⁵ m ² /s ³	2.72·10 ⁻⁵ m ² /s ³	2.22·10 ⁻⁸ m/s ³
potential temperature	338.3 K	0.67 K	0.0105 K/m

G. Discussion

As we present only a few selected cases, one may argue whether these represent rather typical conditions for cruise or not. Vortex lifetimes and descent distances are mainly controlled by thermal stratification (here Brunt-Väisälä

frequency, N) and turbulence energy dissipation rate, ε , which in these cases vary within the limits $0 \leq N \leq 0.02 \text{ s}^{-1}$ and $2 \cdot 10^{-6} \text{ m}^2/\text{s}^3 \leq \varepsilon \leq 5 \cdot 10^{-5} \text{ m}^2/\text{s}^3$, respectively. According to Ref. [15] these ranges of N and ε are well within the range of atmospheric conditions prevailing at cruise altitudes collected from various in situ observations. So, one may conclude that the presented cases are typical for cruise conditions.

The measured initial vortex separations of the Airbus planes are about 15% smaller than those expected from elliptical circulation distribution and 17% smaller for the B744. The presented P2P and P2P^a predictions elucidate that the b_{v0} values have a very strong effect on wake vortex lifetime and descent distance. The spanwise load factor s , which relates the initial vortex separation, b_{v0} , to the wind span, b , according to $s = b_{v0}/b$, amounts to $\pi/4$ for an elliptical spanwise circulation distribution. Here it is briefly discussed how deviations of the load factor from this theoretically ideal value for minimum induced drag may affect wake vortex predictions. The initial circulation $\Gamma_0 = \frac{mg}{\rho s b V}$ is inversely proportional to s , where m is aircraft mass, g gravitational acceleration, ρ is air density, and V is true airspeed. However, the characteristic wake vortex time scale $t_0 = 2\pi \frac{b_0^2}{\Gamma_0}$, which scales with dimensional vortex lifetimes, is proportional to s^3 . So, the descent speed $w_0 = \frac{b_0}{t_0}$ is proportional to s^{-2} . Further, it should be noted that also the effects of the environmental parameters on vortex lifetime depend on s according to $N^* = N t_0$ scaling with s^3 and $\varepsilon^* = \frac{(\varepsilon b_0)^{1/3}}{w_0}$ scaling with $s^{7/3}$. So, with a maximum dependence of these key wake vortex parameters on s^3 , the noticed 15% deviation of the Airbus aircraft may change results by about 40%. For the B744 this impact is even slightly larger. On the other hand, there are also compensating effects of the s -dependences. For example, a large spanwise load factor would on one hand lead to long vortex lifetimes as t_0 becomes large. But at the same time N^* and ε^* also achieve high values, which reduces these increased vortex lifetimes to a certain extent.

This little exposition illustrates the significant relevance of the knowledge of the initial vortex separation for any consideration related to vortex lifetimes and descent distances during cruise. For an onboard wake vortex prediction system [28], it appears crucial to consider these tighter initial vortex separations either by establishing an aircraft type specific data base or by determining average deviations from elliptical spanwise load factors combined with appropriate uncertainties. For approach and landing it would be worthwhile to also know how b_{v0} changes in high-lift conditions. The few measurements available for this phase of flight feature both, b_{v0} values smaller [29] but also partly larger [30] than the values expected from elliptical circulation distributions. Comprehensive measurements of b_{v0} have been accomplished at flight altitudes below 80 m at the London Heathrow airport within the RECAT-EU initiative [31]. Unfortunately, the access to this data is restricted. One reason for the low b_{v0} values is certainly the tradeoff between an elliptical load distribution and a minimization of the wing weight by approving some root loading.

Finally, the presented P2P^a predictions illustrate that for onboard wake vortex predictions with reasonably small wake vortex volumes, which should to be avoided by following aircraft, a good knowledge of the atmospheric wind field is mandatory. Even in the current case where a research aircraft was measuring the wind field, however, in large regions not restricted to where the vortices actually evolved, potentially large wake hazard regions appear unavoidable. At the end of the maximum wake vortex lifetime of the A388 case at $t = 246 \text{ s}$ in Fig. 20, the width of the vertical 95% envelope amounts to about 570 m and the lateral envelope to about 1600 m. The corresponding dimensions of the A359 case in

Fig. 23 at $t = 192 \text{ s}$ are vertically about 500 m and horizontally about 2000 m. For the B744 case shown in Fig. 25 the widths of the probabilistic envelopes amount to about 400 m in vertical direction and to about 1000 m in lateral direction at $t = 155 \text{ s}$, while the predicted probabilistic envelopes were still not wide enough to cover the measurements due to the inhomogeneity of the prevailing wind field. A dedicated reconstruction of the wind field along the aircraft track using wind measurements of the involved aircraft pair, possibly combined with numerical weather prediction data in particular for estimating the respective vertical gradients, may improve the hit rates of the probabilistic predictions and at the same time reduce the dimensions of the wake vortex hazard areas to a size that might be acceptable in terms of the number of wake vortex warnings that would not lead to wake vortex encounters if they were ignored.

VI. Conclusions

Flight data of the trailing vortices of the three aircraft types A380, A359, and B744 has been obtained during cruise flight with the NRC CT-133 research aircraft. Trailing vortex spacing and transport were measured and background atmospheric data derived for input into two versions of the Probabilistic 2-Phase wake vortex prediction model – the ground-based P2P model and its airborne version P2P^a. Vortex circulation estimates were derived from Rankine vortex model fits and from closed-path integrals around the vortices. To the authors' knowledge there are almost no publications dealing with fast-time wake vortex model predictions in cruise conditions. The current paper fills this gap by demonstrating and analyzing the prediction skills of two wake vortex model versions under cruise conditions.

The flight data was obtained in low to moderate turbulence and light to moderate stable thermal stratification. Wind sounding magnitude and direction indicated a level of background atmospheric shear. The degrees of thermal stratification and turbulence energy dissipation rates prevailing during the CT-133 measurements were well within the range of atmospheric conditions collected from various in situ observations at cruise altitudes [15]. As these two parameters mainly control wake vortex lifetimes and descent, the presented cases can be considered typical for wake vortex evolution in cruise conditions.

It is noteworthy that the vortex descent distance measured in the A388 case covers more than 2000 ft and thus about twice the reduced vertical separation minimum (RVSM) of 1000 ft. This means that pilots following or crossing the track of an A388 one flight level below should be aware of the risk of an imminent encounter and should use an upwind flight track whenever possible. The A359 and the B744 cases both illustrate that also the wake vortices generated by other heavy aircraft types may reach down to the next flight level 1000 ft below.

The predictions of two versions of the P2P wake vortex model were compared to the flight data. While the ground-based P2P model failed to predict appropriate probabilistic envelopes mainly for the lateral transport of the wake vortices, the 95%-envelopes predicted by the airborne version P2P^a embraced successfully most of the CT-133 measurement data. Only in one case the wind field was quite inhomogeneous such that the crosswind reconstruction from the CT-133 flight deviated too much from the winds experienced by the wake vortices with the result that the P2P^a predictions didn't match the observations. Also, the circulation estimates were mostly covered well by the probabilistic envelopes of the P2P^a model. The different performances of the P2P and the P2P^a model are expected and related to the different probabilistic model designs. While the established P2P version uses ground-based measurement data to calibrate its probabilistic envelopes [19], the runtime optimized airborne version P2P^a uses uncertainties of all relevant impact parameters to construct the probabilistic envelopes [13]. Ground based measurements may feature substantially higher accuracies than airborne measurements, where the environmental data may be gathered partly in down-track air masses far displaced to those that actually control wake vortex behavior.

Successful predictions of the vortex descent speed and distance by both models require the knowledge of the true initial vortex separation b_{v0} , which was determined by the measurements to be by 15% to 17% smaller than the b_{v0} values expected from elliptical circulation distributions. Such large deviations of the spanwise load factor, s , affect wake vortex prediction results significantly, as key wake vortex parameters have a dependence on s of up to the power of three. The presented cases also demonstrate that the successful prediction of vortex descent has to consider the uncertainty of the flight altitude of the vortex generator. The standard deviation of 31 m derived from estimates by ICAO [24] appears appropriate.

As P2P and P2P^a predict well the average vortex descent speeds and vortex lifetimes and as they employ the same dynamical core, one may conclude that the physics of wake vortex behavior is sufficiently well represented by both P2P model versions. The suitability for either ground-based or airborne applications is mainly connected to the different methods for the consideration of the uncertainties of the aircraft and environmental parameters for the prediction of the probabilistic envelopes.

Provided that reasonable estimates of the input parameters and their uncertainties are available, the P2P^a model appears to be well suited for onboard wake vortex prediction [13]. In order to attain good wake vortex predictions with acceptable dimensions of the probabilistic wake vortex envelopes, a model or database of initial vortex separations should be established and the uncertainties of the crosswind should be minimized. The latter may be

achieved by a dedicated reconstruction of the wind field along the aircraft track using wind measurements of the involved aircraft pair, possibly combined with numerical weather prediction data in particular for estimating the respective vertical gradients.

As next activity flight testing of the wake encounter avoidance and advisory system (WEAA) with the DLR research aircraft ISTAR, a Dassault Falcon 2000LX, is planned for late summer 2025. Automatic Dependent Surveillance - Broadcast (ADS-B) data broadcasted by the wake vortex generating airliners will serve as input for the P2P^a predictions. Traverses of the contrails will be used to validate the predictions of the WEAA system with its P2P^a wake vortex model.

Acknowledgments

The 2006-2021 enroute wake vortex NRC flight research was conducted under the sponsorship of the National Research Council Canada and the Federal Aviation Administration of the United States of America. Part of the development of P2P^a has been performed under contract to Airbus and we gratefully appreciate the support received. The investigations have received funding from the German Aerospace Research Center (DLR) project NICo (Next Generation Intelligent Cockpit).

References

- [1] Hallock, J. N., and Holzäpfel, F., "A Review of Recent Wake Vortex Research for Increasing Airport Capacity", *Progress in Aerospace Sciences*, Vol. 98, 2018, pp. 27-36, <https://doi.org/10.1016/j.paerosci.2018.03.003>.
- [2] Nelson, R. C., "Trailing vortex wake encounters at altitude - A potential flight safety issue?," AIAA Atmospheric Flight Mechanics Conference and Exhibit, AIAA Paper 2006-6268, August 2006, <https://doi.org/10.2514/6.2006-6268>.
- [3] Brown, A. P., "Wake Vortex Considerations in the Analysis of Recorded Data from the Upset to Flight AC190," Rept. LTR-FR-289, National Research Council Canada, Ottawa, Canada, 2008, p. 44.
- [4] Schumann, U., and Sharman, R., "Aircraft wake-vortex encounter analysis for upper levels," *Journal of Aircraft*, Vol. 52, No. 4, 2015, pp. 1277-1285. doi: 10.2514/1.C032909
- [5] Hoogstraten, M., Visser, H. G., Hart, D., Treve, V., and Rooseleer, F., "An improved understanding of en route wake-vortex encounters," *Journal of Aircraft*, Vol. 52, No. 3, 2015, pp. 981-989. doi: 10.2514/1.C032858
- [6] BFU, "Bulletin Unfälle und Störungen beim Betrieb ziviler Luftfahrzeuge, Januar 2017," Bundesstelle für Flugunfalluntersuchung (BFU), Braunschweig, Germany, https://www.bfu-web.de/DE/Publikationen/Bulletins/2017/Bulletin2017-01.pdf?__blob=publicationFile&v=2, January 2017, p. 43.
- [7] Münster, C., and Schwarz, C., "Auswertung von Wirbelschleppenmeldungen im US Aviation Safety Reporting System (ASRS)," Institutsbericht, IB 111-2010/33, Deutsches Zentrum für Luft- und Raumfahrt, Institut für Flugsystemtechnik, Braunschweig, July 2010, p. 17.
- [8] Brown, A.P., "Identification of Trailing Vortex Dynamic States," doi: 10.5772/intechopen.110787, 13th April 2023, from the edited volume "Vortex Simulation and Identification [Working Title]," Dr Chaoqun Liu, published by IntechOpen.
- [9] Vicroy, D.D., Vijgen, P.M., Reimer, H.M., Gallegos, J.L., and Spalart, P.R. , "Recent NASA Wake-Vortex Flight Tests, Flow Physics Database and Wake-Development Analysis," AIAA and SAE, 1998 World Aviation Conference, AIAA Paper 1998-5592, September 1998, <https://doi.org/10.2514/6.1998-5592>.
- [10] Robins, R. E., and Delisi, D. P., "NWRA AVOSS Wake Vortex Prediction Algorithm Version 3.1.1," NASA/CR-2002-211746, June 2002.
- [11] Proctor, F. H., Hamilton, D. W., and Switzer, G. F., "TASS Driven Algorithms for Wake Prediction", AIAA Paper 2006-1073, January 2006, <https://doi.org/10.2514/6.2006-1073>.
- [12] Ahmad, N. N., VanValkenburg, R., Bowles, R., and Limon Duparcmeur, F. M., "Evaluation of Fast-Time Wake Vortex Models using Wake Encounter Flight Test Data", 6th AIAA Atmospheric and Space Environments Conference, AIAA Paper 2014-2466, June 2014, <https://doi.org/10.2514/6.2014-2466>.
- [13] Sölch, I., Holzäpfel, F., Abdelmoula, F., and Vechtel, D., "Performance of on-board wake vortex prediction systems employing various meteorological data sources", *Journal of Aircraft*, Vol. 53, Issue 5, pp. 1505-1516, 2016, <http://arc.aiaa.org/doi/abs/10.2514/1.C033732>.

- [14] Holzäpfel, F., and Gerz, T., "Aircraft Wake Vortices: From Fundamental Research to Operational Application, Research Topics in Aerospace, Atmospheric Physics - Background - Methods - Trends," U. Schumann Editor, Springer, 2012, pp. 219-237, ISBN 978-3-642-30182-7, ISBN 978-3-642-30183-4, <https://doi.org/10.1007/978-3-642-30183-4>.
- [15] Holzäpfel, F., "Effects of Environmental and Aircraft Parameters on Wake Vortex Behavior," *Journal of Aircraft*, Vol. 51, Issue 5, 2014, pp. 1490-1500, <https://dx.doi.org/10.2514/1.C032366>.
- [16] Brown, A.P., and Holzäpfel, F., "Case Studies in Modelling Cruise-generated Trailing Vortices," *AIAA Aviation 2024 Forum*, AIAA Paper 2024-3773, July August 2024, p. 24, <https://doi.org/10.2514/6.2024-3773>.
- [17] Holzäpfel, F., 2003: Probabilistic Two-Phase Wake Vortex Decay and Transport Model, *Journal of Aircraft*, Vol. 40, No. 2, pp. 323-331, <https://doi.org/10.2514/2.3096>.
- [18] Holzäpfel, and F., Robins, R.E., 2004: Probabilistic Two-Phase Aircraft Wake Vortex Model: Application and Assessment, *Journal of Aircraft*, Vol. 41, No. 5, pp. 1117-1126, <https://doi.org/10.2514/1.2280>.
- [19] Holzäpfel, F., 2006: Probabilistic Two-Phase Aircraft Wake-Vortex Model: Further Development and Assessment, *Journal of Aircraft*, Vol. 43, No. 3, pp. 700-708, <https://doi.org/10.2514/1.16798>.
- [20] Holzäpfel, F., and Steen, M., 2007: Aircraft Wake-Vortex Evolution in Ground Proximity: Analysis and Parameterization, *AIAA Journal*, Vol. 45, No. 1, pp. 218-227, <https://doi.org/10.2514/1.23917>.
- [21] Leweke, T., and Le Dizès, S., "Analysis of F/T-1 and F/T-2 LIDAR measurements and smoke visualisations," AWIATOR Technical Report D1.1.4-3 & D1.1.4-11, July 2007, 90 pp.
- [22] Donaldson, C. duP., and Bilanin, A.J., "Vortex Wakes of Conventional Aircraft," NATO, AGARD, AG-204, 1975, Paris.
- [23] Frehlich, R., and Sharman, R., "Estimates of Turbulence from Numerical Weather Prediction Model Output with Applications to Turbulence Diagnosis and Data Assimilation," *Monthly Weather Review*, Vol. 132, No. 10, 2004, pp. 2308–2324. doi:10.1175/1520-0493(2004)132<2308:EOTFNW>2.0.CO;2.
- [24] ICAO, Manual on a 300 m (1 000 ft) Vertical Separation Minimum Between FL 290 and FL 410 Inclusive, International Civil Aviation Organization, Doc 9574, AN/934, 3rd edition, 62 pages, 2012.
- [25] Crow, S. C., "Stability theory for a pair of trailing vortices," *AIAA Journal*, Vol. 8, 1970, pp. 2172–2179, <https://doi.org/10.2514/3.6083>.
- [26] Proctor, F. H., Hinton, D. A., Han, J., Schowalter, D. G., and Lin, Y.-L., "Two-Dimensional Wake Vortex Simulations in the Atmosphere: Preliminary Sensitivity Studies," AIAA Paper 97-0056, January 1997, <https://doi.org/10.2514/6.1997-56>.
- [27] Delisi, D. P., and Robins, R. E., "Effects of Crosswind Shear on Trailing Vortex Evolution," AIAA Paper 2006-1075, 44th AIAA Aerospace Sciences Meeting and Exhibit, January 2006, Reno, Nevada, <https://doi.org/10.2514/6.2006-1075>.
- [28] Bauer, T., Vechtel, D., Abdelmoula, F., and Immisch, T., "In-Flight Wake Encounter Prediction with the Wake Encounter Avoidance and Advisory System," 6th AIAA Atmospheric and Space Environments Conference, AIAA Paper 2014-2333, June 2014, <https://doi.org/10.2514/6.2014-2333>.
- [29] Delisi, D. P., Pruis, M. J., Wang, F. Y., and Lai, D. Y., "Estimates of the Initial Vortex Separation Distance, bo, of Commercial Aircraft from Pulsed Lidar Data", 51st AIAA Aerospace Sciences Meeting, AIAA Paper 2013-0365, January 2013, <https://doi.org/10.2514/6.2013-365>.
- [30] Holzäpfel, F., Vechtel, D., Rotshteyn, G., and Stephan, A., "Plate lines to enhance wake vortex decay for reduced separations between landing aircraft," *Flow: Applications of Fluid Mechanics*, Vol. 2, E6-1 – E6-26, 2022, <https://doi.org/10.1017/flo.2021.16>.
- [31] EUROCONTROL, "European proposal for revised wake turbulence categorisation and separation minima on approach and departure 'RECAT – EU' Safety Case Report," Edition 2.0. Brussels, Belgium: EUROCONTROL, 2017.